Superconductor disks and cylinders in an axial magnetic field: II. Nonlinear and linear ac susceptibilities

Ernst Helmut Brandt
Max-Planck-Institut für Metallforschung, D-70506 Stuttgart, Germany
(Received 14 November 1997)

The ac susceptibility $\chi=\chi'-i\chi''$ of superconductor cylinders of finite length in a magnetic field applied along the cylinder axis is calculated using the method developed in the preceding paper, part I. This method does not require any approximation of the infinitely extended magnetic field outside the cylinder or disk but directly computes the current density J inside the superconductor. The material is characterized by a general current-voltage law $E(J)$, e.g., $E(J)=E_c[J/J_c(B)]^{n(B)}$, where E is the electric field, $B=\mu_0 H$ the magnetic induction, E_c a prefactor, J_c the critical current density, and $n\geqslant 1$ the creep exponent. For $n>1$, the nonlinear ac susceptibility is calculated from the hysteresis loops of the magnetic moment of the cylinder, which is obtained by time integration of the equation for $J(\mathbf{r},t)$. For $n\gg 1$ these results go over into the Bean critical state model. For $n=1$, and for any linear complex resistivity $\rho_{\rm ac}(\omega)=E/J$, the linear ac susceptibility is calculated from an eigenvalue problem which depends on the aspect ratio b/a of the cylinder or disk. In the limits $b/a\ll 1$ and $b/a\gg 1$, the known results for thin disks in a perpendicular field and long cylinders in a parallel field are reproduced. For thin disks in a perpendicular field, at large frequencies $\chi(\omega)$ crosses over to the behavior of slabs in parallel geometry since the magnetic field lines are expelled and have to flow around the disk. The results presented may be used to obtain the nonlinear or linear resistivity from contact-free magnetic measurements on superconductors of realistic shape. [S0163-1829(98)05534-9]

I. INTRODUCTION

In the preceding paper part I (Ref. 1), the current density **J**, magnetic field **B**, and magnetic moment $m(H_a)$ of superconductor cylinders of finite length or disks of arbitrary thickness in an axial magnetic field $B_a(t)=\mu_0 H_a(t)$ (along y) are calculated by time integration of the equation of motion for the circulating current density $J(\mathbf{r},t)$. This method, which does not require any approximation or cutoff of the magnetic field in the infinite space outside the cylinder, generalizes a similar calculation for strips, bars, or slabs in a perpendicular field.[2] The material is characterized by an arbitrary (in general nonlinear) current–voltage law $E(J)$, where E is the electric field, which inside the superconductor is generated by moving Abrikosov vortices. A further assumption, which cannot be relaxed so far, is $\mathbf{B}=\mu_0\mathbf{H}$, which means that the lower critical field B_{c1} of the superconductor and its reversible magnetization $B-\mu_0 H$ are assumed to be zero. This approximation is allowed when B is large enough everywhere in the specimen.

In the present paper the amplitude-dependent ac susceptibility of finite cylinders is calculated from magnetization loops which are computed by the method of part I.[1] In the case of linear resistivity $E/J=\rho_{\rm ac}(\omega)$, the linear ac susceptibility is calculated more elegantly from an eigenvalue problem which depends only on the geometry and therefore yields a general expression into which any linear complex resistivity $\rho_{\rm ac}(\omega)$ may be inserted. Before these two types of susceptibilities are considered in Secs. III and IV, first some exact analytical expressions for both nonlinear and linear ac susceptibilities will be compiled in Sec. II for rings, hollow cylinders, infinite slabs, infinite cylinders, and spheres. The particular case of Ohmic conductors, or superconductors with thermally assisted flux flow (TAFF), is considered in Sec. V. Finally, some concluding remarks are made in Sec. IV.

II. ANALYTICAL ac SUSCEPTIBILITIES

In this section I compile some analytical expressions for nonlinear and linear ac susceptibilities of superconductors and general linear conductors in various geometries. Within the Bean critical state model,[3] the full hysteresis loop of the magnetic moment m in a cycled applied field with amplitude H_0 is completely determined by the virgin magnetization curve $m(H_a)$. One has the general prescription[4–6]

$$m_\downarrow(H_a,H_0)=m(H_0)-2m\left(\frac{H_0-H_a}{2}\right),$$

$$m_\uparrow(H_a,H_0)=-m(H_0)+2m\left(\frac{H_0+H_a}{2}\right), \qquad (1)$$

were $m_\downarrow$ and $m_\uparrow$ are the branches in decreasing and increasing H_a. This construction is independent of the type of time dependence of $H_a(t)$, provided H_a increases and decreases monotonically between the values $\pm H_0$. For sinusoidal $H_a(t)=H_0\sin\omega t$, one may define the nonlinear complex ac susceptibilities $\chi_\mu=\chi'_\mu-i\chi''_\mu$, $\mu=1,2,3,\ldots$,[7]

$$\chi_\mu(H_0,\omega)=\frac{i}{\pi H_0}\int_0^{2\pi} m(t)e^{-i\mu\omega t}d(\omega t). \qquad (2)$$

Usually, the χ_μ are normalized such that for $H_0\to 0$ or $\omega\to\infty$ the ideally diamagnetic susceptibility $\chi(0,\omega)$ results; this normalization is achieved by dividing all χ_μ, Eq. (2), by the magnitude of the initial slope $|m'(0)|$

$=\lim_{H_a\to 0}|\partial m(H_a)/\partial H_a|$. In this paper only the fundamental susceptibility ($\mu=1$) will be considered, denoting χ_1 by χ.

Note that in the critical state model this χ depends only on the amplitude H_0 but not on the frequency ω. For thin circular Bean disks $\chi(H_0)$ was calculated from the magnetization curves of Refs. 6 and 8 in Refs. 6 and 9.

For a thin-walled hollow cylinder and for a narrow planar ring the hysteresis loop is a parallelogram.[4,10,11] This parallelogram applies to planar rings with arbitrary shape, made from flat or round wires, containing no, one, or several weak links, with the weakest one determining the critical current I_c. This is so since at small H_a the screening is perfect and no magnetic flux penetrates the ring or tube. But when H_a exceeds some critical field H_p, the screening current in the ring exceeds the critical value I_c and magnetic flux can leak into the ring such that the circulating current $|I|=I_c$ and the magnetic moment $|m|=m_{\rm sat}$ remain constant. The full parallelogram then follows from Eq. (1) and the complex ac susceptibility of the ring normalized to the initial value $\chi(0)=-1$ is[4]

$$\chi'(h)=-1,$$

$$\chi''(h)=0,\quad h\leqslant 1,$$

$$\chi'(h)=-\frac{1}{2}-\frac{1}{\pi}\arcsin s+\frac{1}{\pi}s\sqrt{1-s^2},$$

$$\chi''(h)=\frac{4}{\pi}\frac{h-1}{h^2}=\frac{1-s^2}{\pi},\quad h\geqslant 1, \tag{3}$$

where $h=H_0/H_p$ and $s=2/h-1$. Note that the dissipation (proportional to χ'') sets in only at amplitudes exceeding the penetration field H_p. The polar plot of Eq. (3), χ'' versus χ' with h as the parameter, is *symmetric*; i.e., $\chi''(\chi')$ yields the same curve as $\chi''(-1-\chi')$.

The ac susceptibilities obtained from the critical state model are *quasistatic*; i.e., they depend only on the amplitude H_0 but not on the frequency. This statement is true even when the critical current density $J_c=J_c(B)$ depends on the local induction and thus Eq. (1) does not apply, e.g., for the magnetization loops computed in Refs. 12,4 and 13 for disks with $J_c(B)=J_c(0)/(1+|B|/B_1)$ (Kim model).

In contrast to these nonlinear quasistatic ac susceptibilities $\chi(H_0)$, the linear ac susceptibilities of materials with linear resistivity, $\rho_{\rm ac}(\omega)$, depend only on the ac frequency but not on the ac amplitude H_0. Examples for this are the Ohmic conductors with real and constant resistivity $\rho_{\rm ac}(\omega)=\rho$, and superconductors in the Meissner state with London's magnetic penetration depth λ, which formally are described by a purely imaginary (nondissipative) resistivity $\rho_{\rm ac}=i\omega\mu_0\lambda^2$. More complicated complex linear resistivities $\rho_{\rm ac}=\rho'+i\rho''$ occur in superconductors with thermally activated depinning above the irreversibility line (or depinning line) in the B-T plane; see, e.g., the models of Refs. 14–20 and the experimentally determined $\rho_{\rm ac}$ in Refs. 19 and 20. In complex notation one usually writes $H_a(t)={\rm Re}\{H_0e^{i\omega t}\}$ where ${\rm Re}\{\cdots\}$ denotes the real part and H_0 is a complex amplitude, e.g., $H_0=-i|H_0|$ if $H_a(t)=H_0\sin\omega t$ is chosen to obtain Eq. (2). The magnetic moment $m(t)$ then formally becomes also complex [the measured moment is ${\rm Re}\{m(t)\}$] and the linear ac susceptibility is then defined as $\chi=\mu-1$,

$$\chi(\omega)=\frac{1}{\pi H_0}\int_0^{2\pi}m(t)e^{-i\omega t}\,d(\omega t). \tag{4}$$

The linear susceptibility $\chi_{\rm ac}(\omega)$ or conductivity $\sigma_{\rm ac}(\omega)=1/\rho_{\rm ac}(\omega)$ is obtained for various geometries by replacing in the analytical expressions for $\chi_{\rm ac}$ the Ohmic resistivity ρ by the complex $\rho_{\rm ac}(\omega)$. For example, by solving the diffusion equation for the magnetic field, with the diffusion constant $D=\rho/\mu_0$ replaced by the complex $D=\rho_{\rm ac}/\mu_0$, one obtains for slabs of width $2a$ in a parallel ac field $H_a(t)=H_0\exp(i\omega t)$ the permeability $\mu=\chi+1=\langle H_{\rm ac}(x,t)\rangle_x/H_a(t)$ and the susceptibility $\chi=\mu-1$,[21,22]

$$\chi_{\rm slab}(\omega)=\frac{\tanh u}{u}-1,\quad u=\frac{a}{\lambda_{\rm ac}}, \tag{5}$$

where

$$\lambda_{\rm ac}=(\rho_{\rm ac}/i\omega\mu_0)^{1/2} \tag{6}$$

is the complex penetration depth or $\rho_{\rm ac}(\omega)=i\omega\mu_0\lambda_{\rm ac}^2$. For a long cylinder with radius a in an axial field one finds[23] for $\chi=\mu-1=\langle H_{\rm ac}(r,t)\rangle_r/H_a(t)-1$,

$$\chi_{\rm cyl}(\omega)=\frac{2I_1(u)}{uI_0(u)}-1,\quad u=\frac{a}{\lambda_{\rm ac}}, \tag{7}$$

with the same $\lambda_{\rm ac}$, Eq. (6); $I_1(u)$ and $I_0(u)$ are modified Bessel functions.

Remarkably, formula (7) applies also to cylinders in transverse field and thus, due to the linearity, to any inclined field $H_a(t)$ forming an angle θ with the cylinder axis. The axial and circulating current components in the tilted infinite cylinder exhibit the same radial dependence $f(r)=(H_a/\lambda_{\rm ac})I_1(r/\lambda_{\rm ac})/I_0(a/\lambda_{\rm ac})$: $J_\parallel=2\cos\varphi\sin\theta f(r)$, $J_\varphi=\cos\theta f(r)$, where φ is the azimuthal angle. The magnetic moment of cylinders in a transverse H_a is twice as large as in a parallel field; this may be ascribed to the demagnetization factor $N=1/2$ or to the contribution of the U turn of the currents at the ends of the cylinder. Thus $|\mathbf{m}|$ contains a factor $(\cos^2\theta+4\sin^2\theta)^{1/2}$, which, however, drops out in the normalized susceptibility (7).

For the sphere one may use London's solution[24] for the magnetic moment of a sphere with radius a in the Meissner state,

$$m=-2\pi H_0a^3\left(1-\frac{3\lambda}{a}\coth\frac{a}{\lambda}+\frac{3\lambda^2}{a^2}\right). \tag{8}$$

Defining $\chi=m(\lambda)/|m(\lambda\to 0)|$ and replacing the real λ by the complex $\lambda_{\rm ac}$, Eq. (6), one obtains the susceptibility of a sphere with arbitrary complex resistivity $\rho_{\rm ac}(\omega)$ and radius a,

$$\chi_{\rm sphere}(\omega)=\frac{3\coth u}{u}-\frac{3}{u^2}-1,\quad u=\frac{a}{\lambda_{\rm ac}}. \tag{9}$$

For the susceptibility of thin disks or strips in perpendicular field, analytical expressions are not available. However, one may express the linear $\chi_{ac}(\omega)$ for any geometry by an infinite sum of the form

$$\chi(\omega)=-w\sum_{\nu}\frac{\Lambda_\nu b_\nu^2}{w+\Lambda_\nu}\Big/\sum_{\nu}\Lambda_\nu b_\nu^2. \tag{10}$$

Here the complex variable w depends on ρ_{ac} and ω and on the geometry, and the dipole moments b_ν and eigenvalues Λ_ν follow from an eigenvalue problem which is different for each geometry; see the examples for thin strips[25,26] and disks[20,25] and thick strips and bars in a perpendicular field,[27] for rectangular bars in a parallel field,[28] and for finite cylinders in an axial field, below in Sec. IV. The sum in the denominator of Eq. (10) provides the normalization $\chi(\omega\to\infty)=-1$ (ideal diamagnetic screening).

For practical purposes, a finite number of terms $\nu=1,\ldots,N$ in the sum (10) is sufficient; cf. Sec. IV. When the (real and positive) numbers Λ_ν and b_ν are known for a given geometry, then $\chi(\omega)$ may be calculated from the sum (10) for any complex resistivity $\rho_{ac}(\omega)$. By inverting this relationship between the two complex functions $\chi(\omega)$ and $\rho_{ac}(\omega)$ numerically, the complex resistivity $\rho_{ac}(\omega)$ may be obtained from measured ac susceptibilities as done by Kötzler *et al.*[20]

III. NONLINEAR ac SUSCEPTIBILITIES

We model the superconductor as a nonlinear conductor with general current-voltage dependence $\mathbf{E}=E(J)\mathbf{J}/J$, e.g., $E(J)=E_c(J/J_c)^n$ with arbitrary creep exponent $n\geqslant 1$. In addition; $\mathbf{B}=\mu_0\mathbf{H}$ is assumed, see the discussion in Sec. V of part I.[1] The nonlinear resistivity for $n\gg 1$ is caused by thermally activated depinning with an activation energy $U(J)=U_0\ln(J_c/J)$ yielding a creep exponent $n=U_0/kT$; see Sec. III D of part I. In axial symmetric geometry, i.e., for cylindrical specimens in an axial magnetic field along $\hat{\mathbf{y}}$, the currents, electric field, and vector potential are directed along $\hat{\varphi}$, where $\varphi=\mathrm{atan}(z/x)$, namely, $\mathbf{J}=J(r,y,t)\hat{\varphi}$, $\mathbf{E}=E(r,y,t)\hat{\varphi}$, and $\mathbf{A}=A(r,y,t)\hat{\varphi}$. In particular, the applied field is now $\mathbf{B_a}=B_a(t)\hat{\mathbf{y}}=\nabla X(A_a\hat{\varphi})$ with $A_a=-(r/2)B_a$. The components of the magnetic field are $B_r=\partial A/\partial y$ and $B_y=-(1/r)\partial(rA)/\partial r$. During our computation of J and m, B_r and B_y do not have to be calculated except when one assumes a B-dependent current-voltage law, e.g., of the form $E(J,B)=E_c[J/J_c(B)]^{n(B)}$. In general, $E(J,B_r,B_y)$ may depend on both components of $\mathbf{B}$, e.g., when $J_c(B_r,B_y)$ is anisotropic like in c-axis-oriented cylinders of uniaxial high-T_c superconductors. Our method applies also to these anisotropic materials.

The equation of motion for the current density $J(r,y,t)$ in cylinders or disks is given in part I.[1] On a two-dimensional (2D) grid of N points $\mathbf{r}_i=(r_i,y_i)(i=1,\ldots,N)$ spanning the quarter cross section $0\leqslant r\leqslant a$, $0\leqslant y\leqslant b$ (or half cross section $0\leqslant r\leqslant a$, $-b\leqslant y\leqslant b$ if the specimen has no symmetry plane at $y=0$) this equation of motion reads

$$\mu_0\dot{J}_i(t)=\sum_j R_{ij}\left[E(J_j)-\frac{1}{2}r_j\dot{B}_a\right]. \tag{11}$$

Here the vector $J_i(t)=J(\mathbf{r}_i,t)$ and the applied field $B_a(t)$ depend on the time t, $E(J)$ is a given function, e.g., $E=J^n$ in reduced units, and $R_{ij}=(Q_{ij}w_j)^{-1}$ is a reciprocal matrix into which enters the matrix $Q_{ij}=Q(\mathbf{r}_i,\mathbf{r}_j)$ defined in part I and the weights w_i of the grid points (e.g., $w_i=ab/N$ for equidistant grids). Throughout this paper, for increased accuracy I use nonequidistant grids which are denser (and have thus smaller weights) near the cylinder surface.

Equation (11) is easily time integrated by starting at time $t=0$ with $B_a=0$ and $J_i=0$ and then increasing the applied field $B_a(t)$ to obtain the solution $J_i(t)$. From the current density $J_i(t)$ the magnetic moment $m(t)$ of the cylinder (directed along y like B_a) is obtained as

$$m(t)=2\pi\int_0^a dr\ r^2\int_0^b dy\ J(r,y,t)=2\pi\sum_{i=1}^{N} r_i^2 J_i(t)w_i. \tag{12}$$

In this section $B_a(t)=\mu_0 H_0\sin\omega t$ is chosen; the nonlinear ac susceptibility then follows from Eq. (2).

The resulting magnetization loops $m(B_a(t))$ become stationary shortly after 1/4 cycle or even earlier; i.e., the transition from the virgin curve to the final hysteresis loop occurs rapidly (see Figs. 14–17 in part I). This is a consequence of the nonlinear $E(J)$ relation; in the Ohmic case with $E\propto J$ the transient time is somewhat larger and the stationary loop is reached exponentially in time. For exponents $n\geqslant 2$ it is thus sufficient to calculate χ from the half loops in the time interval $0.55\pi\leqslant\omega t\leqslant 1.55\pi$.

Without restriction of generality we may choose the circular frequency $\omega=1$ corresponding to $\omega=E_c/(\mu_0 J_c a^2)$ when reduced units $a=J_c=E_c=\mu_0=1$ are used. The scaling law of part I, Sec. III E, states that when a material law $E\propto J^n$ is assumed, then the susceptibility $\chi(H_0,\omega)$ depends only on combinations of the form $H_0/\omega^{1/(n-1)}$ or ω/H_0^{n-1} or on any function of these ratios. Therefore, the $\chi(H_0,\omega)$ for different frequencies ω are obtained by rescaling the amplitude axis. For example, one has $\chi(H_0,10\omega)=\chi(10^{1/(n-1)}H_0,\omega)$. This scaling to a good approximation applies also to other $E(J)$ laws if these are sufficiently nonlinear and if the effective exponent n is defined as $n=\partial(\ln E)/\partial(\ln J)$ taken at $J=J_c$ where J_c is the typical current density of the experiment. The nonlinear susceptibility thus depends only on *one* variable combining amplitude and frequency, further on the effective exponent n, and on the geometry expressed, e.g., by the aspect ratio b/a of the cylinder.

Figures 1–6 show the nonlinear susceptibilities $\chi(H_0,\omega)$ at $\omega=E_c/(\mu_0 J_c a^2)$ for various geometries, for creep exponents $n=3$, 5, 11, 51, and for constant J_c and B-dependent $J_c(B)$, using various types of plots. The real and imaginary parts of $\chi=\chi'-i\chi''$ of cylinders with half length to radius ratio $a/b=3$, 0.3, and 0.03 in an axial magnetic field are plotted in Fig. 1 versus $\log(H_0/H_p)$, in Fig. 3 versus H_0/H_p, and in Fig. 5, χ'' is plotted versus $-\chi'$ (polar plot). Here H_0 is the amplitude of the applied ac field $H_a(t)=H_0\sin\omega t$ and H_p is the field where full penetration occurs in the Bean model. For bars in a perpendicular field and cylinders in an axial field, both with rectangular cross sections $2a\times 2b$, one has[2,29]

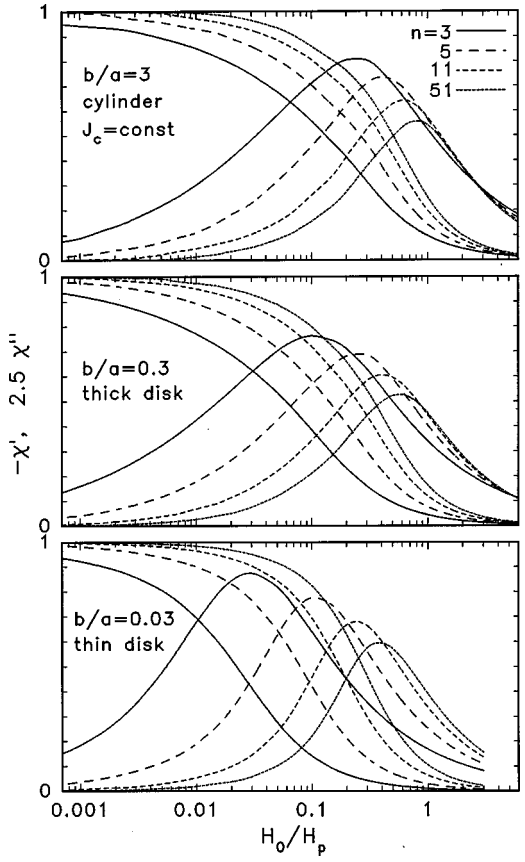

FIG. 1. Nonlinear magnetic susceptibility $\chi(H_0,\omega)=\chi'-i\chi''$ of cylinders with aspect ratios $a/b=3$, 0.3, and 0.03 in an axial ac magnetic field with frequency $\omega=E_c/(\mu_0 J_c a^2)$ and amplitude H_0 referred to the field of full penetration H_p, Eq. (14) ($H_p/J_c a=0.9824$, 0.5757, 0.1260 for $b/a=3$, 0.3, 0.03). Depicted is χ' (monotonic curves) and χ'' (curves with maximum) on a semilogarithmic plot for creep exponents $n=3$ (solid lines), $n=5$ (long dashed lines), $n=11$ (medium dashed lines), and $n=51$ (short dashed lines) for constant J_c. The curves $n=51$ are close to the Bean limit.

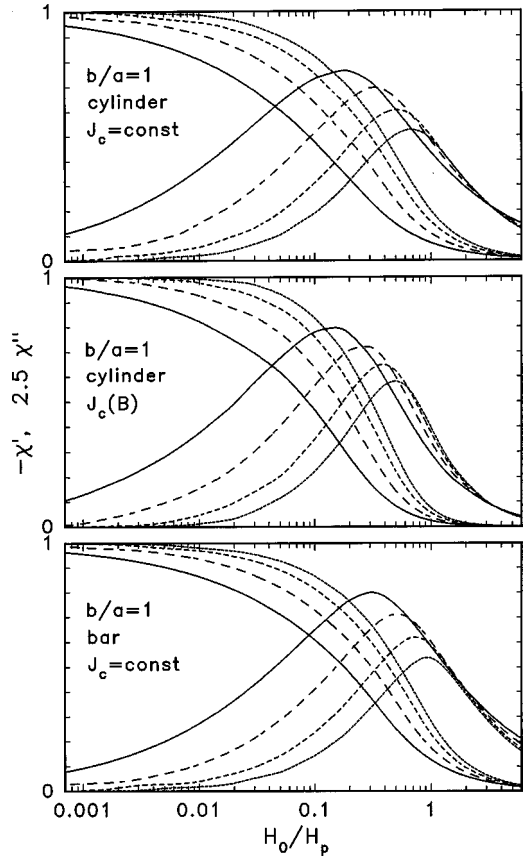

FIG. 2. Similar as in Fig. 1 but for a cylinder with $b/a=1$ and $J_c=\text{const}$ (top, $H_p/J_c a=0.8814$), $J_c(B)=J_c(0)/(1+2B/\mu_0 H_p)$ (middle, Kim model), and for a bar with $b/a=1$ and $J_c=\text{const}$ (bottom, $H_p/J_c a=0.7206$). Four creep exponents $n=3$, 5, 11, and 51 are shown, as in Fig. 1.

$$H_p=J_c\frac{b}{\pi}\left[\frac{2a}{b}\arctan\frac{b}{a}+\ln\left(1+\frac{a^2}{b^2}\right)\right] \quad \text{(bar)}, \tag{13}$$

$$H_p=J_c b\ln\left[\frac{a}{b}+\left(1+\frac{a^2}{b^2}\right)^{1/2}\right] \quad \text{(cylinder)}. \tag{14}$$

This gives $H_p/J_c a=0.9824$ (0.8814, 0.5757, 0.1260) for cylinders with $b/a=3$ (1, 0.3, 0.03), and $H_p/J_c a=0.7206$ for a bar with $b/a=1$. In Figs. 2, 4, and 6 similar χ' and χ'' are plotted for a cylinder with $b/a=1$ and $J_c=\text{const}$ or $J_c(B)=J_c(0)/(1+2B/\mu_0 H_p)$ (Kim model) with $B=|\mathbf{B}(x,y)|$, and for a bar with $b/a=1$. Note that the depicted curves look qualitatively similar for all six cases. The slight oscillation of some of the curves with large b/a is an artifact due to a too small number N_x of grid planes along x (or cylinders along r); e.g., in these figures nonequidistant grids were used with $N_x=9$, $N_y=20$ for $b/a=3$ and $N_x=30$, $N_y=3$ for $b/a=0.03$.

In the Bean limit $n\to\infty$, the general behavior of χ' and χ'' at small and large amplitudes H_0 is explicitly known. Expanding the virgin magnetization curve at small H_0,

$$M(H_0)=\alpha H_0+\beta H_0^2+\gamma H_0^3+\cdots, \tag{15}$$

one obtains, from Eqs. (1) and (2) $\chi=\chi'-i\chi''$,

$$\chi'(H_0)=\alpha+\beta H_0+\frac{15}{16}\gamma H_0^2+\cdots, \tag{16}$$

$$\chi''(H_0)=\frac{4}{3\pi}\beta H_0+\frac{2}{\pi}\gamma H_0^2+\cdots. \tag{17}$$

In particular, using the virgin curves of part I, Sec. II, one obtains the following relations. For long cylinders and slabs in a parallel field the coefficients in Eq. (15) are $\alpha<0$, $\beta>0$, and $\gamma\leqslant 0$; thus when χ is normalized to $\chi(H_0=0)=-1$, both $1-|\chi'|$ and χ'' start linearly with a term $\propto\beta H_0/|\alpha|$. This result applies also to our numerically obtained $\chi(H_0)$ of cylinders of finite lenght. Thus, in the polar plots of Figs. 5 and 6, the curves $\chi''(-\chi')$ start linearly in the lower right corner. Explicitly one has, up to terms linear in $h_0=H_0/H_p$ in longitudinal geometry,

$$\chi(H_0)=-1+\frac{1}{2}h_0-i\frac{2}{3\pi}h_0+\cdots \quad \text{(slab)}, \tag{18}$$

$$\chi(H_0)=-1+h_0-i\frac{4}{3\pi}h_0+\cdots \quad \text{(cylinder)}. \tag{19}$$

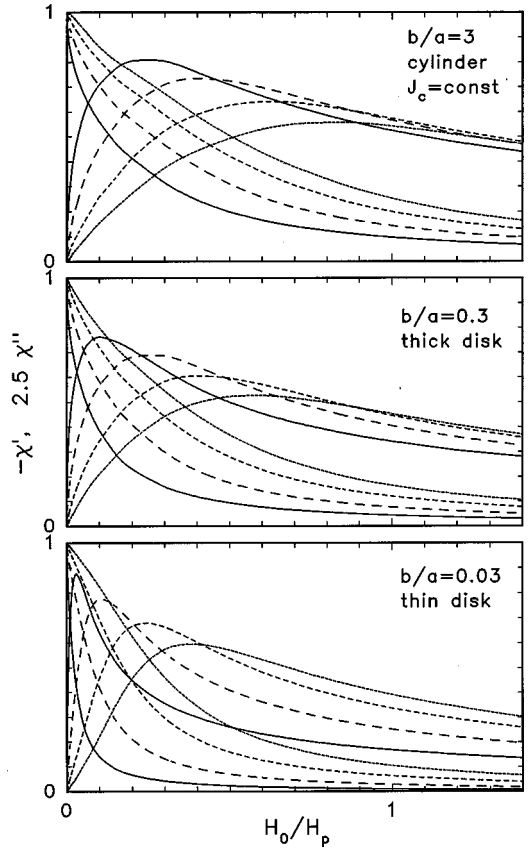

FIG. 3. As in Fig. 1 but with a linear abscissa.

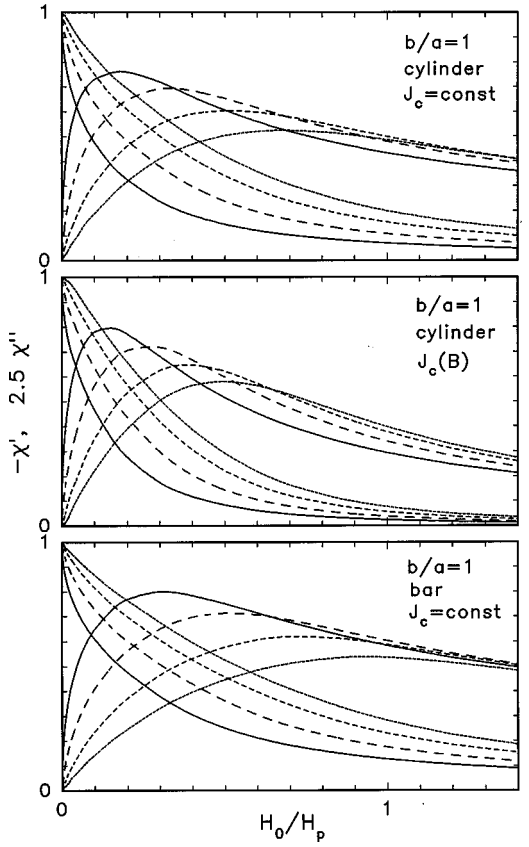

FIG. 4. As in Fig. 2 but with a linear abscissa.

For thin strips and disks in a perpendicular field one has $\alpha<0$, $\beta=0$, and $\gamma>0$; i.e., there is no quadratic term in the virgin magnetization curve [cf. Eqs. (11) and (14) in part I]. Explicitly, for the thin strip one has $m(H_a)\propto\tanh(h)=h-h^3/3+O(h^5)$ with $h=H_a/H_s$ and $H_s=2J_cb/\pi$; thus $\beta=0$ and $\gamma=-\alpha/(3H_s^2)$. For the thin disk the expansion of the bracket in Eq. (11) of part I yields $2h-h^3+O(h^5)$ with $h=H_a/H_d$ and $H_d=J_cb$; thus $\beta=0$ and $\gamma=-\alpha/(2H_d^2)$. With these γ/α values the small-amplitude expansion of χ yields

$$\chi(H_0)=-1+\left(\frac{5}{16}-\frac{2i}{3\pi}\right)\frac{H_0^2}{H_s^2}+O(H_0^4)\ \text{(strip)}, \quad (20)$$

$$\chi(H_0)=-1+\left(\frac{15}{32}-\frac{i}{\pi}\right)\frac{H_0^2}{H_d^2}+O(H_0^4)\ \text{(disk)}. \quad (21)$$

The slope of $\chi''(-\chi')$ in the lower right corner of Figs. 5 and 6 in the Bean limit should thus take the universal values

$$\left.\frac{\chi''}{1+\chi'}\right|_{\chi''\to 0}=\begin{cases}4/3\pi=0.42 & \text{for } \beta\neq 0,\\ 32/15\pi=0.68 & \text{for } \beta=0,\end{cases} \quad (22)$$

where the case $\beta=0$ corresponds to thin films in a perpendicular magnetic field and $\beta\neq 0$ to all other geometries. These slopes are approximately reached in the depicted case $n=51$, but for stronger creep ($n=11,\ 5,\ 3$) the slopes are larger. Note also that our assumption $B=\mu_0H$ requires that

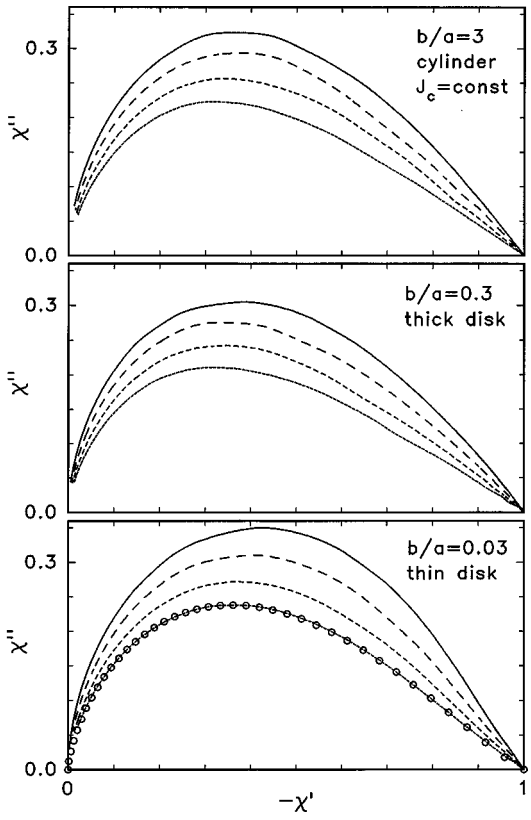

FIG. 5. The data of Fig. 1 plotted as χ'' vs $-\chi'$. The open circles in the lower plot show the fit, Eq. (24).

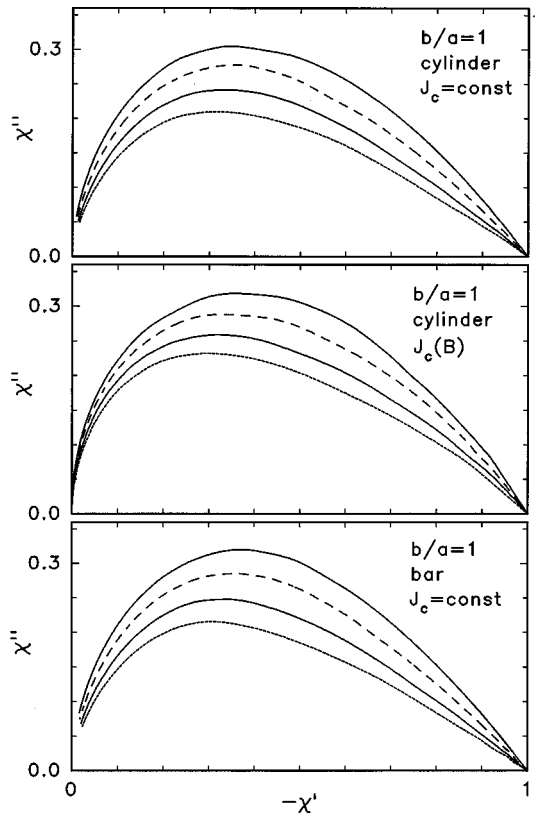

FIG. 6. The data of Fig. 2 plotted as χ'' vs $-\chi'$.

the amplitudes be not too small, $H_0 \gg H_{en}$, where H_{en} is the field above which the penetrating vortices can overcome the geometric edge barrier.[31,32]

At large amplitudes $H_0 \gg H_p$ the magnetization loop in the Bean limit may be approximated by a parallelogram for all geometries. Therefore, $\chi(H_0)$ is given by expressions of the type of Eq. (3); see also Ref. 10. In the limit $H_0 \gg H_p$ one has then $\chi'(H_0) \propto H_0^{-3/2}$ and $\chi''(H_0) \propto H_0^{-1}$. The curves $\chi''(-\chi')$ in Figs. 5 and 6 in the lower left corners thus behave as

$$\chi'' = \text{const} \times |\chi'|^{2/3}. \tag{23}$$

For all computed cylinders in the Bean limit we find for the constant in Eq. (23) the value 0.80. A very good fit for all values of $0 \leqslant -\chi' \leqslant 1$ for the cylinder with $b/a = 0.03$ in the Bean limit is

$$\chi'' \approx 0.80 |\chi'|^{2/3} (1 - |\chi'|)^{1.19}, \tag{24}$$

depicted as dots in the lower plot of Fig. 5. Similar fits are possible for the other cylinders and the bar, but for strong creep ($n \leqslant 11$) and nonconstant $J_c(B)$ the limit (23) does not apply.

IV. LINEAR ac SUSCEPTIBILITIES

If the resistivity $\rho = E/J$ of the material is linear, the magnetic response is also linear and may be expressed in the most general form by a linear complex susceptibility $\chi(\omega)$ which depends on the linear complex ac resistivity $\rho_{\rm ac}(\omega)$. In this case it is not necessary to time integrate the equation of motion (11) containing the inverse kernel R_{ij}. One may directly solve the original equation for the current density in a bar [Eq. (6) or (44) in Ref. 2] or cylinder [Eq. (24) in Ref. 1]. Inserting the periodic time dependences $H_a(t) = H_0 e^{i\omega t}$, $J(\mathbf{r},t) = J(\mathbf{r}) e^{i\omega t}$, and $E(\mathbf{r},t) = E(\mathbf{r}) e^{i\omega t}$, where now formally H_0, $J(\mathbf{r})$, and $E(\mathbf{r}) = \rho_{\rm ac}(\omega) E(\mathbf{r})$ are complex amplitudes [as usual, the physical quantities are obtained by taking the real part of $H_a(t)$, $J(\mathbf{r},t)$, and $E(\mathbf{r},t)$], one obtains, for the cylinder in an axial ac magnetic field the integral equation for $J(\mathbf{r})$,

$$\frac{\rho_{\rm ac}(\omega)}{i\omega\mu_0} J(\mathbf{r}) = \int_S Q_{\rm cyl}(\mathbf{r},\mathbf{r}') J(\mathbf{r}')\, d^2r' + \frac{r}{2} H_0. \tag{25}$$

Here $\mathbf{r} = (r,y)$, $\mathbf{r}' = (r',y')$, and $S = ab$ is the integration area (a quarter of the clinder cross section $2a \times 2b$). The kernel $Q_{\rm cyl}(\mathbf{r},\mathbf{r}')$ is defined by Eq. (21) of part I. Equation (25) is related to the eigenvalue problem

$$f_\nu(\mathbf{r}) = -\Lambda_\nu \frac{4\pi}{S'} \int_0^a dr' \int_0^b dy'\, Q_{\rm cyl}(\mathbf{r},\mathbf{r}') f_\nu(\mathbf{r}'), \tag{26}$$

with positive eigenvalues Λ_ν and real eigenfunctions $f_\nu(r,y)$, $\nu = 1,2,\ldots,\infty$. For cylindrical symmetry we may normalize the $f_\nu(\mathbf{r})$ as[25]

$$\frac{4\pi}{S'} \int_0^a dr\, r \int_0^b dy\, f_\mu(\mathbf{r}) f_\nu(\mathbf{r}) = \delta_{\mu\nu}. \tag{27}$$

(A different normalization introducing the symmetric kernel $Q(\mathbf{r},\mathbf{r}')\sqrt{r/r'}$ is used in Ref. 30.) The arbitrary area S' in Eqs. (26) and (27) was introduced to make the Λ_ν and f_ν dimensionless. Natural choices of S' are[7,27] $S' = S = 4ab$ in the limit $b \gg a$ (long cylinder) and $S' = 16a^2/\pi$ in the limit $b \ll a$ (thin disk); see below.

Expanding $J(\mathbf{r})$ into a series of the eigenfunctions,

$$J(\mathbf{r}) = \sum_\nu a_\nu f_\nu(\mathbf{r}), \tag{28}$$

we obtain from Eqs. (25)–(28) the magnetic moment $m(t) = m(\omega) e^{i\omega t}$, Eq. (12),

$$m(\omega) = 2\pi \int_0^a dr\, r^2 \int_0^b dy\, J(r,y) = \frac{S'}{2} \sum_\nu a_\nu b_\nu, \tag{29}$$

where we have defined the ''oscillator strengths''

$$b_\nu = \frac{4\pi}{S'} \int_S r^2 f_\nu(r,y)\, d^2r. \tag{30}$$

Multiplying Eq. (25) by $f_\mu(\mathbf{r})$ and integrating $\mathbf{r}$ over S on both sides using formulas (26) and (27), one obtains the expansion coefficients

$$a_\nu = H_0 \frac{2\pi}{S'} \frac{w\Lambda_\nu}{w + \Lambda_\nu} b_\nu \tag{31}$$

and the magnetic moment (29) becomes

$$m(\omega) = H_0 \pi w \sum_\nu \frac{\Lambda_\nu b_\nu^2}{w + \Lambda_\nu}. \tag{32}$$

The results (31) and (32) depend on the complex variable

$$w=\frac{i\omega\mu_0 S'}{4\pi\rho_{\rm ac}(\omega)}=\frac{S'}{4\pi\lambda_{\rm ac}^2}=i\omega\tau(\omega), \tag{33}$$

which combines the complex resistivity $\rho_{\rm ac}(\omega)$ with the frequency ω and with the arbitrary area S' appearing also in the definitions (26), (27), and (30). This w may also be written in terms of the complex penetration depth $\lambda_{\rm ac}=(i\omega\mu_0/\rho_{\rm ac})^{1/2}$; cf. the variable $u=a/\lambda_{\rm ac}$ in Eqs. (59), (7), and (9).

With formula (33) we may express the linear ac susceptibility $\chi(\omega)=-m(\omega)/m(\omega\to\infty)=\mu(\omega)-1$ of cylinders in axial field in the form of Eq. (10),

$$\chi(\omega)=-\sum_\nu \frac{wc_\nu}{w+\Lambda_\nu},\quad \mu(\omega)=\sum_\nu \frac{c_\nu\Lambda_\nu}{w+\Lambda_\nu}, \tag{34}$$

$$c_\nu=\Lambda_\nu b_\nu^2\Big/\sum_\nu \Lambda_\nu b_\nu^2. \tag{35}$$

Here w is the variable (33), Λ_ν are the eigenvalues of Eq. (26), and b_ν are the integrals (30) over the eigenfunctions of Eq. (26). The normalization in Eq. (35) guarantees that for $\omega\to\infty$ one has $\chi\to-\Sigma_\nu c_\nu=-1$ and $\mu\to0$, irrespective of the values of Λ_ν and b_ν. With the Λ_ν and b_ν computed from Eqs. (26), (27), and (30), the limit $m(\omega\to\infty)$ exactly coincides with the ideal diamagnetic moment of cylinders $m'(0)$, Eq. (42) of part I. Sum rules for the b_ν^2, $b_\nu^2\Lambda_\nu$, and b_ν^2/Λ_ν for thin strips and disks are given in Ref. 25.

Examples for the normalized amplitudes c_ν and eigenvalues (or pole positions) Λ_ν are given in Table I for cylinders with aspect ratios $b/a=0.15$, 0.3, 1, and 3. For this Table I chose $S'=4ab$; thus one has $\tau(\omega)=\mu_0 ab/[\pi\rho_{\rm ac}(\omega)]$ in Eq. (33). The grids $\mathbf{r}_i=(r_i,y_i)$ were chosen to be nonequidistant (denser near the cylinder surface) as decribed below Eq. (29) of part I. For transparency a constant number of grid points was used, $N=N_x\times N_y=36$ with $N_x\times N_y=12\times3$, 9×4, 6×6, and 4×9. The obtained Λ_ν and c_ν were sorted for increasing Λ_ν; at large ν these positive numbers are very sensitive to the choice of the grid, but the resulting $\chi(\omega)$ is less sensitive. The $\chi(\omega)$ calculated from Table I are valid from $\omega=0$ up to at least $\omega\tau=200$. For higher frequencies more grid points are required. At extreme aspect ratios $b/a\ll1$ and $b/a\gg1$ the $N\times N$ matrix $Q_{ij}=Q_{\rm cyl}(\mathbf{r}_i,\mathbf{r}_j)$ (cf. part I) of the eigenvalue problem may become singular, or some of the eigenvalues artificially may turn out to be negative, depending on the choice of the grid.

The finite number N of grid points results in the same finite number of eigenvalues, $\nu=1,2,\ldots,N$. At small b/a a nearly equidistant series of Λ_ν results, which is typical for thin strips and disks in a perpendicular field; see Eqs. (48) and (49) below. The rapid increase of the Λ_ν as the index ν approaches N is an artifact caused by the finite N. With increasing aspect ratio b/a, Λ_ν and c_ν arrange in groups which for $b/a\to\infty$ degenerate and coincide with the result for the long cylinder; cf. Eq. (47) below.

TABLE I. Eigenvalues Λ_ν (sized) and amplitudes c_ν entering the general linear ac susceptibility $\chi(\omega)$, Eq. (34), of cylinders with radius a and length $2b$ in an axial magnetic field. In all three examples nonequidistant grids with $N=N_x\times N_y=36$ points were used, with $N_x\times N_y=12\times3$, 9×4, 6×6, and 4×9 for $b/a=0.15$, 0.3, 1, and 3. For this table $S'=4ab$ was used, which means $\tau(\omega)=\mu_0 ab/[\pi\rho_{\rm ac}(\omega)]$ in Eq. (33).

b/a	0.15		0.3		1		3	
ν	Λ_ν	10^3c_ν	Λ_ν	10^3c_ν	Λ_ν	10^3c_ν	Λ_ν	10^3c_ν
1	1.125	610.3	1.371	590.2	2.561	575.8	6.127	590.9
2	3.092	125.6	4.391	129.1	7.710	53.58	9.108	50.49
3	5.900	54.63	9.261	59.10	11.17	116.2	13.91	17.64
4	9.621	30.98	14.03	32.31	17.59	17.83	20.44	8.587
5	14.25	20.16	16.16	25.20	18.66	9.554	28.19	6.187
6	19.62	14.67	18.71	9.800	27.56	53.78	33.44	128.4
7	25.19	31.03	24.80	23.23	29.66	2.400	36.57	5.350
8	25.85	0.168	25.05	0.044	34.43	7.138	37.04	2.437
9	29.11	6.139	32.63	2.847	35.31	2.601	42.72	4.352
10	30.66	0.224	33.48	2.780	46.28	4.477	49.99	2.179
11	33.52	5.880	39.55	14.81	47.22	4.409	52.73	3.018
12	35.39	7.806	41.88	6.768	50.32	9.523	57.75	1.385
13	38.75	2.176	48.22	0.206	55.43	0.222	66.18	1.254
14	44.43	2.054	51.02	9.942	63.20	0.032	71.81	11.35
15	50.27	1.658	57.45	1.860	65.29	40.67	77.27	6.078
16	56.57	2.473	57.86	0.903	65.67	5.003	80.52	1.519
17	57.29	10.15	64.38	1.557	67.29	0.089	83.57	1.334
18	60.20	0.017	72.33	1.287	74.23	0.003	85.14	0.000
19	67.40	2.413	80.59	1.495	78.85	0.002	90.22	0.142
20	91.61	1.188	84.38	23.46	80.83	1.564	94.89	0.040
21	129.2	24.75	86.91	0.002	87.21	1.963	104.6	4.555
22	141.6	10.22	94.39	0.442	97.66	0.781	107.4	0.444
23	170.6	0.443	108.3	1.607	101.8	1.166	140.1	1.943
24	171.1	0.006	143.6	1.618	112.3	0.090	160.6	0.214
25	193.6	2.257	213.5	18.31	133.8	1.630	190.5	63.31
26	213.1	0.223	272.8	0.203	300.5	52.28	234.6	13.07
27	229.9	0.771	318.6	2.432	321.4	2.736	266.6	29.39
28	242.1	0.481	355.7	1.198	407.0	5.490	292.1	12.37
29	251.1	0.079	375.6	0.411	409.3	0.009	316.0	15.08
30	269.6	0.000	441.7	0.070	467.4	12.17	340.1	0.735
31	293.0	0.000	470.1	23.89	471.0	0.755	348.6	5.622
32	314.4	0.000	512.5	0.000	555.9	11.35	396.1	1.890
33	322.9	2.335	569.6	0.000	562.8	0.004	552.6	6.473
34	824.8	16.36	659.1	4.704	674.7	0.000	843.4	0.652
35	1114.0	0.965	840.1	4.733	707.3	5.585	895.7	1.585
36	2483.0	11.33	897.2	3.531	794.4	3.173	1280.0	0.003

V. OHMIC AND TAFF RESISTIVITY

In the Ohmic case or for thermally assisted flux flow (TAFF) (Ref. 22) in superconductors, the resistivity $\rho_{\rm ac}=\rho=1/\sigma$ is real and independent of ω. Therefore, the time constant $\tau=\mu_0 S'/(4\pi\rho)$ in Eq. (33) is also real and constant and the variable $w=i\omega\tau$ is purely imaginary. With the choice $S'=4ab$ one then has $\tau=\mu_0 ab\sigma/\pi$ and $w=i\omega\mu_0 ab\sigma/\pi$.

For Ohmic conductivity the time τ has the following physical meaning. When the applied field is suddenly switched on or off at time $t=0$, the current density $J(\mathbf{r},t)$ at $t\geq0$ may be expressed as a linear superposition of relaxing eigenmodes,

$$J_\nu(\mathbf{r},t)=f_\nu(\mathbf{r})e^{-t/\tau_\nu}. \tag{36}$$

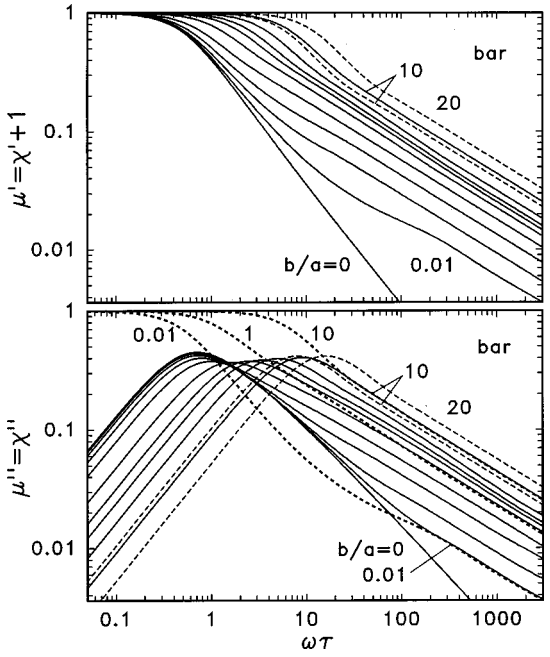

FIG. 7. The real part (top) and imaginary part (bottom) of the ac permeability $\mu=\chi-1=\mu'-i\mu''$ for Ohmic bars with rectangular cross section $2a\times 2b$ in a perpendicular magnetic ac field for aspect ratios $b/a=0$ (thin strip), $b/a=0.01$, 0.03, 0.1, 0.3, 1, 2, 3, 5, and 10 as computed from the sum (34) (solid lines). The dashed curves give the analytic expressions (5) for long slabs with $b/a=5$ and 10, with the variable $u=a/\lambda_{ac}=(i\omega\tau\pi a/b)^{1/2}$ inserted. For $b/a=10$ the numerical and analytical curves are very close. To facilitate comparison, some μ' curves are repeated as dotted lines in the lower plot. The time scale is $\tau=\mu_0 ab/(\pi\rho)$.

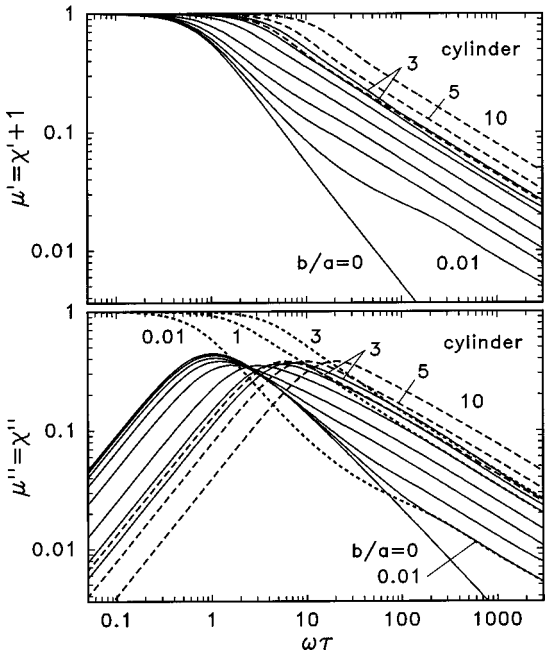

FIG. 8. As in Fig. 7, but for Ohmic cylinders in axial magnetic ac field and for $b/a=0$ (thin disk), $b/a=0.01$, 0.03, 0.1, 0.3, 1, 2, and 3 as computed from the sum (34) (solid lines), and for $b=3$, 5, and 10 from the analytical expression (7) for longitudinal cylinders (dashed lines). The numerical and analytical curves for $b/a=3$ are very close.

Here $f_\nu(\mathbf{r})$ are the eigenfunctions of Eq. (26) (or of another equation for different geometry) and the $\tau_\nu=\tau/\Lambda_\nu$ are relaxation times depending on the eigenvalues Λ_ν. In particular, for thin strips (disks) one has (choosing $S'=4ab$)[25] $\Lambda_1=0.638\,523$ (0.876 827) and $\Lambda_\nu\approx\Lambda_1+\nu-1$ for all $\nu=1,2,\ldots,\infty$. In general, the relaxation times are given by[2] $\tau_\nu=\mu_0 S'/(4\pi\rho\Lambda_\nu)$. For long slabs ($b\gg a$) in a parallel field, the eigenvalues of Eq. (26) are $4\pi\Lambda_\nu/S'=\pi^2(\nu-\frac{1}{2})^2/a^2$. For $S'=4ab$ this gives $\Lambda_\nu=(\nu-\frac{1}{2})\pi b/a$, but the different choice $S'=16a^2/\pi$ in this geometry yields more natural (size-independent) values $\Lambda_\nu=(2\nu-1)^2=1,\ 9,\ 25,\ldots$.

Figures 7–10 show the linear ac susceptibility $\chi=\chi'-i\chi''=\mu-1$ or permeability $\mu=\mu'-i\mu''=\chi+1$ of Ohmic bars and cylinders of various aspect ratios, calculated from Eq. (34) as a function of the frequency $\omega/2\pi$. In these plots the time unit is $\tau=\mu_0 ab/(\pi\rho)$ where ρ is the Ohmic resistivity. This τ means that $S'=4ab$ was chosen. Thus, for $b\ll a$ the plotted $\chi(\omega\tau)$ is independent of b/a (except at very large frequencies; see below), but for $b\gg a$ the $\chi(\omega\tau)$ curves depend on b such that $\chi(\omega\tau a/b)$ becomes a universal function. This invariance may be seen from the expressions (5) and (7) for $\chi(\omega)$ of long slabs and cylinders in a parallel field, which depend on the variable $u=a/\lambda_{ac}=(a^2 i\omega\mu_0/\rho)^{1/2}$. In our time unit τ this becomes $u=(i\omega\tau\pi a/b)^{1/2}$; thus χ for $b\gg a$ becomes a universal function of the variable u or of the combination $\omega\tau a/b$. In this longitudinal limit a more natural choice of the time unit would thus be $\tau_{long}=(4a^2\mu_0/\pi\rho)$ corresponding to a choice $S'=16a^2/\pi$ in the general expression $\tau=\mu_0 S'/(4\pi\rho)$. If desired, a function $\tilde{\tau}(a,b)$ may be fitted such that for all ratios a/b the Ohmic $\chi''(\omega\tilde{\tau})$ exhibit their maximum at the same position. Alternatively, $\tilde{\tau}(a,b)$ may be chosen such that the initial slope of $\chi''(\omega\tilde{\tau})$ becomes unity for all a/b;

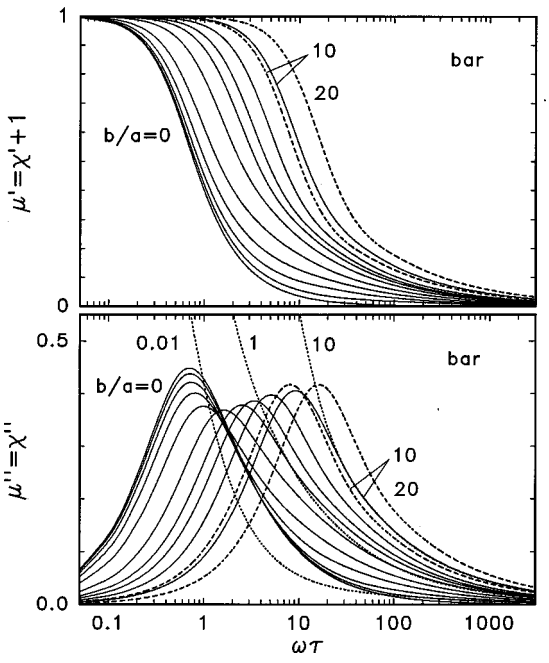

FIG. 9. As in Fig. 7 but with a linear abscissa.

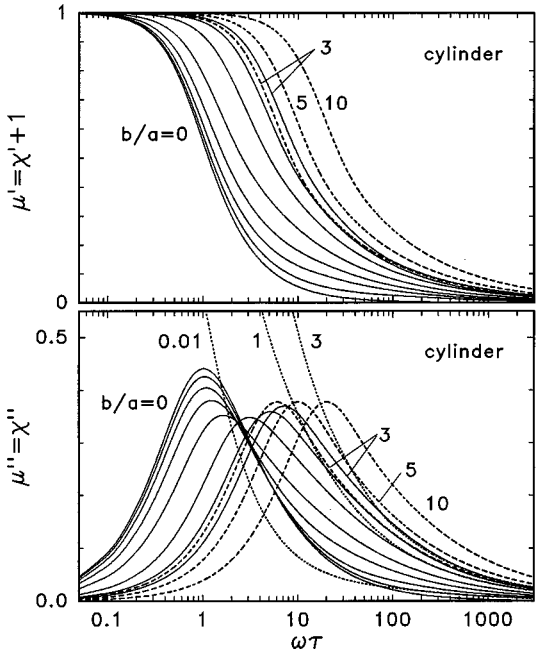

FIG. 10. As in Fig. 8 but with a linear abscissa.

see Eqs. (39) and (42) below. With both choices the resulting curves $\chi'(\omega\tilde{\tau})$ and $\chi''(\omega\tilde{\tau})$ for all b/a will nearly coincide; see Fig. 11 below.

Figure 7 shows the real and imaginary parts of the ac permeability $\mu=\mu'-i\mu''=\chi-1$ for Ohmic bars with rectangular cross section $2a\times 2b$ in a perpendicular magnetic ac field for aspect ratios $b/a=0$ (thin strip), $b/a=0.01$, 0.03, 0.1, 0.3, 1, 2, 3, 5, and 10, as computed from the sum (34). Also shown in this plot are the analytic expressions (5) for long slabs with $b/a=5$ and 10, with the variable $u=a/\lambda_{ac}=(i\omega\tau\pi a/b)^{1/2}$ inserted. Note that the numerical and analytical $\mu(\omega\tau)$ for $b/a=10$ nearly coincide.

The corresponding ac permeabilities for Ohmic cylinders in axial magnetic ac field are shown in Fig. 8 for $b/a=0$

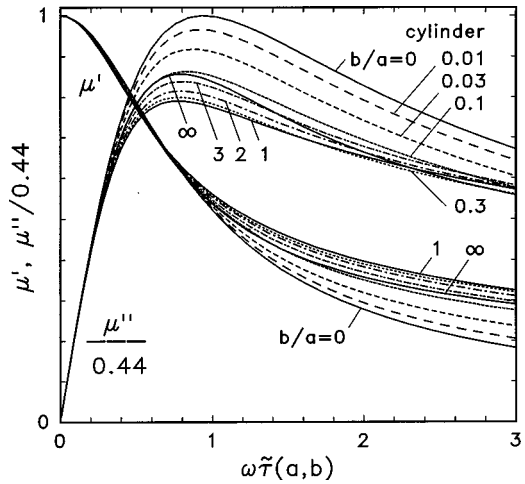

FIG. 11. The linear ac susceptibilities of cylinders in axial field from Figs. 8 and 10, plotted vs $\omega\tilde{\tau}(a,b)$ such that the initial slope $d\chi''/d(\omega\tilde{\tau})$ is unity for all plotted values $b/a=0$, 0.01, 0.03, 0.1, 0.3, 1, 2, 3, and ∞. The time unit $\tilde{\tau}(a,b)$ is given by Eq. (42).

(thin disk), $b/a=0.01$, 0.03, 0.1, 0.3, 1, 2, and 3 as computed from the sum (34), and for $b=3$, 5, and 10 from the analytical expression (7) for longitudinal cylinders. Again the numerical and analytical curves for $b/a=3$ are very close. Note also that bars and cylinders behave very similarly, but for cylinders the longitudinal limit is reached at lower values of a/b.

The most interesting feature in these double-logarithmic plots is that for sufficiently thin specimens with increasing frequency $\mu(\omega)$ crosses over from the behavior in perpendicular geometry (nonlocal flux diffusion),[25]

$$\mu'=\chi'+1\propto 1/\omega, \quad \mu''=\chi''\propto \ln(\text{const}\times\omega\tau)/\omega, \quad (37)$$

to the parallel geometry (local flux diffusion),

$$\mu'\approx\mu''\propto 1/\sqrt{\omega}. \quad (38)$$

This crossover is clearly seen with the curves $b/a=0.01$, 0.03, and 0.1 in Figs. 7 and 8. One furthermore realizes that for all aspect ratios b/a, except for the limit $b=0$, the real and imaginary parts at large frequencies coincide, $\mu'(\omega)=\mu''(\omega)$. The physical reason for this finding is that above the frequency where the skin depth $\delta=\sqrt{2}\lambda_{ac}=(2\rho/i\omega\mu_0)^{1/2}$ coincides with the half thickness b, the Ohmic conductor nearly behaves like an ideal diamagnet (or superconductor in the Meissner state), screening almost all magnetic flux from the interior of the conductor. The magnetic field lines thus cannot penetrate into the bulk but have to flow around the bar or cylinder such that everywhere **B** is *parallel* to the specimen surface. Therefore, at high frequencies even thin conductors (whether Ohmic or non-Ohmic) in a perpendicular ac field *behave as if the magnetic field were applied parallel*.

Figures 9 and 10 show the same data as Figs. 7 and 8 but with a linear ordinate. This presentation clearly shows that with increasing specimen thickness the height of the maximum of $\chi''(\omega)$ (i.e., of the energy dissipation) goes through a minimum at $b/a\approx 1$.

In Fig. 11 the susceptibility of Ohmic cylinders with various lengths is plotted such that the initial slope of $\chi''(\omega)$ is normalized to unity. This is achieved by introducing an appropriate time unit $\tilde{\tau}(a,b)$. The plotted $\chi'(\omega\tilde{\tau})$ and $\chi''(\omega\tilde{\tau})$ then look qualitatively similar for all aspect ratios a/b. An analytical expression for the time $\tilde{\tau}(a,b)$ may be found in the following way. From the definition $\chi(\omega)=m(\omega)/m(\omega\to\infty)=\chi'-i\chi''$ and the small-frequency behavior $\chi=-i\omega\tilde{\tau}-\beta\omega^2+\cdots$, where β is a positive constant, one sees that this time constant $\tilde{\tau}=\partial\chi''/\partial\omega|_{\omega=0}$ may be written as

$$\tilde{\tau}(a,b)=\frac{-m(\omega\to 0)}{i\omega m(\omega\to\infty)}. \quad (39)$$

The magnetic moment $m(\omega)$ of an Ohmic cylinder in the limit of *low frequencies* is obtained noting that in this limit the magnetic field penetrates completely; thus the electric field is

$$E(\mathbf{r},t)=\frac{r}{2}\dot{B}_a(t)=\frac{r}{2}i\omega\mu_0 H_a(t) \quad (40)$$

and the current density is $J(\mathbf{r},t)=E(\mathbf{r},t)/\rho$. With the definition (12) the magnetic moment of the cylinder at low frequencies then becomes

$$m(\omega\to 0)=\frac{\pi b a^4}{4\rho}i\omega\mu_0 H_a(t). \tag{41}$$

The magnetic moment at *high frequencies* is that of an ideal diamagnet since in this limit the magnetic field is completely screened from the interior of the specimen by the skin effect. One has $m(\omega\to\infty)=m'(0)H_a(t)$ where $m'(0)\approx-(2\pi b a^2+8a^3/3)$ is the initial slope of the virgin magnetization curve given by Eq. (43) of part I. With the above-defined $\tau=\mu_0 ab/(\pi\rho)$ one may thus write for the initial slope of $\chi''(\omega)$ of cylinders

$$\tilde{\tau}=\frac{(3\pi^2/32)\tau}{1+3\pi b/4a+\frac{1}{2}\tanh[1.27(b/a)\ln(1+a/b)]}. \tag{42}$$

This $\tilde{\tau}(a,b)$ and the corresponding area $S'=4\pi\rho\tilde{\tau}/\mu_0$ have the limits $\tilde{\tau}/\tau=3\pi^2/32\approx 1$, $S'=3\pi^2 ab/8$ for $b/a\ll 1$ and $\tilde{\tau}/\tau=\pi a/(8b)$, $S'=\pi a^2/2$ for $b/a\gg 1$.

From Fig. 11 one sees that for all ratios b/a the dissipative part $\chi''(\omega)$ has its maximum close to $\omega=1/\tilde{\tau}$. More precisely, for $b/a=0$, 0.01, 0.03, 0.1, 0.3, 1, 2, 3, and ∞ one has $\chi''_{\max}=\chi''(\omega_{\max})=0.4406$, 0.4256, 0.4045, 0.3803, 0.3521, 0.3482, 0.3591, 0.3694, and 0.3774 occurring at $\omega_{\max}\tilde{\tau}=0.948$, 0.918, 0.877, 0.832, 0.779, 0.779, 0.792, 0.805, and 0.794.

VI. CONCLUDING REMARKS

For long slabs and cylinders ($b\gg a$) in a parallel field the eigenvalues Λ_ν and eigenfunctions $f_\nu(\mathbf{r})$ may be derived directly from a differential equation with boundary conditions for the magnetic induction $\mathbf{B}=B\hat{\mathbf{y}}$. Namely, from the Maxwell equations $\mathbf{J}=\nabla\times\mathbf{H}$ (neglecting the displacement current), $\dot{\mathbf{B}}=-\nabla\times\mathbf{E}$, $\nabla\cdot\mathbf{B}=0$, and the material equations $\mathbf{E}=\rho\mathbf{J}$ and $\mathbf{B}=\mu_0\mathbf{H}$ one obtains the diffusion equation

$$\dot{\mathbf{B}}(\mathbf{r},t)=\frac{\rho}{\mu_0}\nabla^2\mathbf{B}(\mathbf{r},t). \tag{43}$$

Inserting here the periodic time dependence $e^{i\omega t}$ one obtains the eigenvalue equation $(i\omega\mu_0/\rho)\mathbf{B}(\mathbf{r})=\nabla^2\mathbf{B}(\mathbf{r})$. For the slab geometry with boundary conditions $B'(0)=B(a)=0$ for $B(x)$ along y, one finds that the solution of this linear diffusion problem is a linear superposition of eigenfunctions $g_\nu(x)$ of the eigenvalue problem

$$g_\nu(x)''=-k_\nu^2 g_\nu(x),\quad g'_\nu(0)=g_\nu(a)=0. \tag{44}$$

This is solved by $g_\nu(x)=\cos k_\nu x$ with $k_\nu=(\nu-\frac{1}{2})\pi/a$, $\nu=1,2,3,\ldots$. The current density along z now is $J(x)=B'(x)/\mu_0$, and the eigenvalues of the differential equation (44) for $B(x)$ and integral equation for $J(x)$ [Eq. (25) with the kernel $Q_{\rm cyl}$ replaced by the kernel $Q_{\rm sym}$ of Ref. 2] obey the identity[2] $4\pi\Lambda_\nu/S'=k_\nu^2$.

Similarly, for long cylinders in a parallel field Eq. (43) leads to a diffusion equation for $B(r,t)$ in cylindrical coordinates. The corresponding eigenvalue problem is

$$g_\nu(r)''+\frac{g'_\nu(r)}{r}=-k_\nu^2 g_\nu(r),\quad g'_\nu(0)=g_\nu(a)=0. \tag{45}$$

This is solved by $g_\nu(r)=J_0(k_\nu r)$ where $J_0(\rho)$ is a Bessel function and the $k_\nu=\rho_{0\nu}/a$ are related to the zeros of $J_0(\rho)$, $\rho_{0\nu}=2.405$, 5.520, 8.634, ... for $\nu=1,2,3,\ldots$. One has approximately[33] $\rho_{0\nu}\approx\pi(\nu-\frac{1}{4})+(1/8\pi)/(\nu-\frac{1}{4})$. Thus, the eigenvalues $\Lambda_\nu=k_\nu^2 S'/4\pi$ for the long slab and cylinder are

$$\Lambda_\nu=\left(\nu-\frac{1}{2}\right)^2\frac{\pi S'}{4a^2}\quad\text{(slab)}, \tag{46}$$

$$\Lambda_\nu\approx\left(\nu-\frac{1}{4}\right)^2\frac{\pi S'}{4a^2}\quad\text{(cylinder)}. \tag{47}$$

The eigenfunctions for the current densities $J(x)=B'(x)/\mu_0$ and $J(r)=B'(r)/\mu_0$ of the long slab and cylinder are $f_\nu(x)=\sin k_\nu x$ and $f_\nu(r)=J_1(k_\nu r)$ where $J_1(\rho)=-J_0'(\rho)$ is another Bessel function. From these solutions f_ν and Λ_ν one may, after some lengthy calculation, reproduce the closed-form expressions (5) and (7) for the linear ac susceptibility $\chi(\omega)$ by evaluating the sum (34) analytically.

For thin strips and disks ($b\ll a$) in a perpendicular field the eigenvalues Λ_ν of Eq. (26) are approximately linear functions of the index ν,[25]

$$\Lambda_\nu\approx(\nu-1+0.6385)\frac{S'}{4ab}\quad\text{(strip)}, \tag{48}$$

$$\Lambda_\nu\approx(\nu-1+0.8768)\frac{S'}{4ab}\quad\text{(disk)}. \tag{49}$$

The formulas (46)–(49) show that $S'=16a^2/\pi$ and $S'=4ab$ are natural choices for S' in the parallel and perpendicular geometries, respectively, since they yield Λ_ν values that are independent of the specimen width $2a$ and length $2b$ and start with lowest eigenvalues which are of order unity, namely, $\Lambda_1=1$ ($2.344\approx 9/4$, 0.6385, 0.8768) for the slab (cylinder, strip, disk). The eigenfunctions $f_\nu(x)$ and $f_\nu(r)$ for the thin strip and disk look similar as in the parallel geometry; see Fig. 2 in Ref. 20.

For more complicated geometries like cylinders of finite length, closed-form expressions for the linear susceptibility $\chi(\omega)$ are not available, and all the more not for the nonlinear susceptibilities. One thus has to use sums of the form (34) with numerically obtained numbers c_ν and Λ_ν; see Table I.

The explicit expressions (5), (7), (9), (10), and (34) for $\chi[\omega,\rho_{\rm ac}(\omega)]$ are very useful since they apply to arbitrary linear complex resistivity, including the Ohmic and TAFF (Ref. 22) cases $\rho_{\rm ac}(\omega)=\rho=1/\sigma$ and the Meissner state described by the London equation, in which formally $\rho_{\rm ac}(\omega)=i\omega\mu_0\lambda^2$ where λ is the London penetration depth. By in-

verting such a relationship between χ and ρ_{ac} numerically, one may extract the linear complex resistivity from measurements of the ac susceptibility as was done in Ref. 20. In the nonlinear case one has to fit or compare the measured χ to the computed $\chi(H_0)$ or $\chi(H_0,\omega)$ as was done, e.g., in Refs. 6–13,34, and 35.

ACKNOWLEDGMENTS

Stimulating discussions with P. Esquinazi, P. Ziemann, J. Gilchrist, A. Gurevich, L. Prigozhin, J. Kötzler, J.R. Clem, and M.V. Indenbom are gratefully acknowledged. This work was supported by the German-Israeli Foundation for Research and Development, Grant No. I-300-101.07/93.

[1] E. H. Brandt, preceding paper [Phys. Rev. B **58**, 6506 (1998) (referred to as part I)].
[2] E. H. Brandt, Phys. Rev. B **54**, 4246 (1996).
[3] C. P. Bean, Phys. Rev. Lett. **8**, 250 (1962); Rev. Mod. Phys. **36**, 31 (1964).
[4] E. H. Brandt, Phys. Rev. B **55**, 14 513 (1997).
[5] A. M. Campbell and J. E. Evetts, Adv. Phys. **21**, 199 (1972).
[6] J. Zhu, J. Mester, J. Lockhart, and J. Turneaure, Physica C **212**, 216 (1993).
[7] R. W. Rollins and J. Silcox, Phys. Rev. **155**, 404 (1967); H. J. Fink, *ibid.* **161**, 417 (1967); D. de Klerk and C. A. M. van der Klein, J. Low Temp. Phys. **6**, 1 (1972); T. Ishida, R. B. Goldfarb, S. Okayasu, Y. Kazumata, J. Franz, T. Arndt, and W. Schauer, Mater. Sci. Forum **137-139**, 103 (1993).
[8] P. N. Mikheenko and Yu. E. Kuzovlev, Physica C **204**, 229 (1993).
[9] J. R. Clem and A. Sanchez, Phys. Rev. B **50**, 9355 (1994).
[10] T. Ishida and H. Mazaki, J. Appl. Phys. **52**, 6798 (1981).
[11] J. Gilchrist and M. Konczykowski, Physica C **212**, 43 (1993).
[12] E. H. Brandt, Physica C **235-240**, 2939 (1994).
[13] J. McDonald and J. R. Clem, Phys. Rev. B **53**, 8643 (1996).
[14] M. Coffey and J. R. Clem, Phys. Rev. Lett. **67**, 386 (1991).
[15] E. H. Brandt, Phys. Rev. Lett. **67**, 2219 (1991).
[16] A. E. Koshelev and V. M. Vinokur, Physica C **173**, 465 (1991).
[17] D. S. Fisher, M. P. A. Fisher, and D. A. Huse, Phys. Rev. B **43**, 130 (1991).
[18] A. T. Dorsey, Phys. Rev. B **43**, 7575 (1991).
[19] R. Behr, J. Kötzler, A. Spirgatis, and M. Ziese, Physica A **191**, 464 (1992).
[20] J. Kötzler, G. Nakielski, M. Baumann, R. Behr, F. Goerke, and E. H. Brandt, Phys. Rev. B **50**, 3384 (1994).
[21] E. H. Brandt, Rep. Prog. Phys. **58**, 1465 (1995).
[22] P. H. Kes, J. Aarts, J. van der Berg, C. J. van der Beek, and J. A. Mydosh, Supercond. Sci. Technol. **1**, 242 (1989).
[23] E. Maxwell and M. Strongin, Phys. Rev. Lett. **10**, 212 (1963); J. R. Clem, H. R. Kerchner, and T. S. Sekula, Phys. Rev. B **14**, 1893 (1976).
[24] F. London, *Superfluids II. Macroscopic Theory of Superconductivity* (Dover, New York, 1961), p. 35.
[25] E. H. Brandt, Phys. Rev. B **50**, 13 833 (1994).
[26] E. H. Brandt and A. Gurevich, Phys. Rev. Lett. **76**, 1723 (1996).
[27] E. H. Brandt, Phys. Rev. Lett. **76**, 4030 (1996).
[28] E. H. Brandt, Phys. Rev. B **50**, 4034 (1994).
[29] A. Forkl, Phys. Scr. **T49**, 148 (1993).
[30] A. Gurevich and E. H. Brandt, Phys. Rev. B **55**, 12 706 (1997).
[31] N. Morozov, E. Zeldov, D. Majer, and B. Khaykovich, Phys. Rev. Lett. **76**, 138 (1996); C. J. van der Beek, M. V. Indenbom, G. D'Anna, and W. Benoit, Physica C **258**, 105 (1996); E. H. Brandt (unpublished).
[32] E. Zeldov, A. I. Larkin, V. B. Geshkenbein, M. Konczykowski, D. Majer, B. Khaykovich, V. M. Vinokur, and H. Shtrikman, Phys. Rev. Lett. **73**, 1428 (1994); M. V. Indenbom and E. H. Brandt, *ibid.* **73**, 1731 (1994); E. Zeldov, A. I. Larkin, M. Konczykowski, B. Khaykowich, D. Majev, V. B. Geshkenbein, and V. M. Vinokur, Physica C **235-240**, 2761 (1994); I. L. Maksimov and A. A. Elistratov, Pis'ma Zh. Éksp. Teor. Fiz. **61**, 204 (1995) [JETP Lett. **61**, 208 (1995)].
[33] *Handbook of Mathematical Functions*, edited by M. Abramowitz and I. A. Stegun (Dover, New York, 1965), p. 371.
[34] F. Mrowka, M. Wurlitzer, P. Esquinazi, E. H. Brandt, M. Lorenz, and K. Zimmer, Appl. Phys. Lett. **70**, 898 (1997).
[35] Th. Herzog, H. A. Radovan, P. Ziemanmn, and E. H. Brandt, Phys. Rev. B **56**, 2871 (1997).